APPENDICES

APPENDIX A

A.1 Literature reviews of Sn-doped ZnO films

Materials	Method	Conclusion	Reference
ZnO (0.1 M solution of zinc acetate in a mixture of ethanol and deionized water, in a volume proportion of 3:1) doped with Sn (tin tetrachloride).	Spray pyrolysis	Tested sensitivity of ethanol vapor (at 435 and 675 K; 40 ppm and at 675 K; 4−100 ppm) in air. Changes in the conductivity as a function of temperature suggest that their magnitude is determined by three basic mechanisms: electron activation, oxygen adsorption, and oxygen desorption. It is shown that doped ZnO thin films deposited with a spray pyrolysis system can have high sensitivity to ethanol vapor (as high as 190). Sn and Al dopants gave the highest sensitivity in the working temperature of 675 K.	[75]

The atomic percentages of dopant in solution were X/Zn = 1, 3, 5, 7, 10 and 15 at%			
Sn-doped ZnO films with 0.1−0.3 M $ZnCl_2$ and 2–4% $SnCl_2$ used as precursors	Spray pyrolysis	The films deposited onto bare glass and onto ITO coated glass substrates are polycrystalline and show a peak that fit with the (002) diffraction peak of the zinc oxide wurtzite structure. The averaged grain size visualized by SEM is around 0.1–0.2 μm, which is quite higher than the crystallite size deduced from the full width at half maximum (FWHM). The Sn-doped ZnO films show the best electrical conductivity. The conductivity is 2–3 orders of magnitude higher after annealing, while the transmission of the annealed ZnO films decreases strongly in the near IR domain. Such modification of the transmission properties of the film testifies of the	[76]

		presence of a high concentration of mobile electrons in the crystallites of the film.	
Sn-doped ZnO films using 0.2 M $ZnCl_2$ and $SnCl_4$ as precursors (with Sn concentration ~0.5−3 at%)	Two-stage chemical deposition (TSCD) process	Addition of more than 1.5% Sn as a dopant induces poisoning of the nucleation stage and hinders the formation of fine ZnO grains. With a nodular-shape dense appearance, the film produced from zinc containing complex having 1.5% Sn as precursor, is composed of even sized ZnO particles of 110–190 nm from SEM micrographs. The resistivity decreases with the increasing of the doping amount of tin. It can be concluded that the optimum concentration of Sn dopant in producing thin films containing fine grains with little resistivity is about 1.5%. The optical energy gap (E_g) increases with the increasing of the doping amount of Sn in zinc oxide films. The value of E_g ranges from 3.05 to 3.18 eV depending on the amount of Sn incorporated.	[78]
0−6.0 at% tin (Sn)-doped ZnO films with zinc	Spray pyrolysis	X-ray diffraction analysis indicates that the deposited films were polycrystalline and oriented to the substrate surface (*c*-axis orientation). From electron probe microanalysis (EPMA) analysis, it is shown that tin-doped ZnO films are nearly	[81]

chloride and tin chloride as precursors		stoichiometric. Tin-doped films with 2 at% show the dense and less porous structure than undoped ZnO. From XPS results, the binding energy of Zn2p is 1022 eV, which corresponds to results from previous studies of zinc bonded as ZnO. The binding energy of Sn3d5/2 is 486.4 eV corresponding to that in SnO_2, his on their concentrations is more important in bulk. The optical transmission of about 85% with resistivity as low as 5×10^{-2} Ω-cm has been related for as deposited doped films. The decrease in optical transmission in IR range, which may be explained by the increase of free carrier concentration which passes from 1.7×10^{17} to 3×10^{18} cm^{-3}, due to the improvement of crystallinity after annealing.	
Sn concentration on zinc oxide (ZnO) film with various Sn concentrations in	Ultrasonic spray pyrolysis (USP)	The XRD patterns showed that the as-deposited films have polycrystalline structure. The crystalline nature of the films was deteriorated with increasing Sn concentration and a shift to amorphous structure was seen. Besides, the preferential orientation of ZnO films also changed, the half peak widths increased and grain sizes decreased depending on the increasing Sn concentration. The effect of Sn concentration was to	[82]

the solution (Sn/Sn+Zn ratio from 0 to 50 at%) at a substrate temperature of 350°C		increase the surface roughening and change considerably the morphologies of ZnO films. ZnO:Sn films are composed of mixed crystallites of ZnO wurtzite, cubic Zn_2SnO_4 and tetragonal SnO_2 structures. The resistivity of ZnO films decreases for lower Sn concentration (at 10%) and then increases for higher Sn concentration (at 30–50%). It was determined from the *I-V* plots that ZnO and ZnO:Sn (at 50%) films have deep trapped structures, ZnO:Sn (at 10%) films have ohmic structure and ZnO:Sn (at 30%) films have shallow trapped structure. Depending on the increasing Sn concentration, donor like trap energy (E_t) values of ZnO films decreased and activation energy (E_a) values of ZnO films increased. Consequently, they suggested that ZnO and ZnO:Sn (at 10%) films may use as antireflecting coating and window material in solar cells due to their low resistivity and higher transparency in the visible range. The other films may be used in gas sensors where high conductivity is unnecessary.	
Sn-doped ZnO	Novel	On SEM-EDX results, the crystallites have the mean sizes around 200 nm for Sn-	[83, 192]

thin films with $ZnSO_4$ and sodium stannate used as precursors (with 4−7 at% of Sn concentrations)	successive ionic layer adsorption and reaction (SILAR)	doped ZnO. Electrical resistivity measurements showed semiconducting nature with room temperature resistivity 1.5×10^5 and 70 Ω-cm for as-deposited ZnO and 4 at% Sn-doped ZnO, respectively. The sensitivity was tested toward NO_2 and NH_3 in air at room temperature and up to 250°C in the concentrations of 1–1.5 ppm and 100 ppm, respectively. 4 at% Sn-doped ZnO thin film sensor showed higher sensitivity than pure ZnO for NO_2 gas (Sensitivity = ~9, at 150°C, 1 ppm). The response and recovery times of the sensor for 1 ppm NO_2/dry air mixture were about 20 and 25 min, respectively. The sensitivity is higher for sensors on the Sn-doped ZnO rapid photothermal processing (RPP) processed at 550°C and 650°C, 15 s, respectively.	
Tin-doped ZnO thin films with zinc sulphate and Na_2SnO_3 as precursors	Successive ionic layer adsorption and reaction (SILAR)	On SEM-EDS results, the crystallites of the deposited material are visible in the as-grown film and have the sizes around 200 nm. The observed particle size of the films processed with rapid photothermal temperature at 650°C varies between 0.2 and 0.5 μm. The sensitivity of NO_2 (50−150°C; 0.5−1.5 ppm) was tested in air. The best condition for Sn-doped ZnO sensor toward NO_2 was at 5 at% of Sn concentration,	[84]

	technique and rapid photothermal processing (RPP)	150°C, 1.5 ppm, 11 of sensitivity. It was experimentally demonstrated that tin impurities in ZnO films improved sensors gas-sensing properties to NO_2 and produce a shorter response time. These experimental results confirm that conductometric gas sensors based on tin-doped ZnO as sensitive layer are of great interest for NO_2 detection.	
Sn-doped ZnO thin films using zinc acetate dihydrate and $SnCl_4$ as precursors (with 1−10 at% of Sn concentration)	Sol-gel	The undoped and low percentage Sn-doped films have (002) as the preferred orientation. The grain sizes from XRD of the ZnO:Sn thin films with 0, 2 and 4 at% Sn concentration were estimated to be ~23, ~16.2 and ~11.5 nm, respectively. The HRTEM results of the undoped films show that the crystallite size of the ZnO film is in the ~20–25 nm range (marked by white lines). The crystallite sizes from TEM of the ZnO:Sn thin films with the 2 and 4 at% Sn concentrations are ~10 to 20 nm and ~8 to 10 nm, respectively. The ethanol sensing test on the ethanol concentration and working temperature was performed in the range of 0−400 ppm and 200−300°C, respectively. The best response (~150), the shortest response time (~40 s) and	[85]

		recovery time (~60 s) to 300 ppm of ethanol was observed for the sample with the 4 at% Sn concentration at a temperature of 250°C.	
ZnO (0.1 M solution of zinc acetate in a mixture of ethanol and deionized water, in a volume proportion of 3:1) doped with Sn (tin tetrachloride). The atomic percentage of	Spray pyrolysis	For Sn-doped films the preferred orientation (POQ_{hkl}) tendency of the films as a function of dopant concentration is similar, it is observed a sharp increase of the POQ_{002} for very slightly doped films (~0.1−0.2 at% Sn/In) then there is a plateau just to 0.7 at%. The average grain size of Sn-doped ZnO film in the range of 0 to 0.8 at%, calculated using Scherrer's formula, is in the range of 22 to 34 nm, respectively. Typical morphology of 5−10 at% Sn-doped ZnO film reveals medium fake-like with basal plane (BP). High resolution electron microscopy (HREM) image of undoped ZnO films deposited onto sodium chloride crystals. It can be clearly observed that grains are formed by many small crystallites aggregates with sizes varying between 6 and 12 nm.	[187]

dopant in solution were X/Zn = 1, 3, 5, 7, 10 and 15 at%.			
Pure and Sn-doped ZnO films (with Sn concentrations up to 16%)	Pulse laser deposition (PLD)	The specific resistivity is found to increase and the transmission of visible light to decrease with increasing Sn concentration. For Sn doping we have fabricated films with Sn concentrations up to c=0.17 measured by X-ray photoelectron spectroscopy (XPS).	[188]
ZnO:Sn with zinc acetate dehydrate and tin chloride as the sources	Sol–gel	Undoped and doped films regardless of dopants and their doping concentrations had only a (002) diffraction peak, indicating the preferred grain growth along the (002) plane. For tin doped films, particles with different shapes and sizes were mixed, and only almost-round grains were observed without columnar shaped grains. The lowest electrical resistivity value of doped films with a second-heat treatment was 5.6×10^{-2}	[189]

		Ω-cm for Sn. The lower transmittance in tin doped films may be due to the increase in optical scattering caused by the mixing of small and large particles as well as its rough surface morphology.	
0−6.0 at% tin (Sn)-doped ZnO films with zinc chloride and tin chloride as precursors	Spray pyrolysis	The preferred (002) growth orientation of the films is not affected while an improvement of the material crystallinity is observed with this dopant. From SEM image, undoped film depicts a microstructure consisted of hexagonal-like grain of approximately 200 nm size. Whereas Sn-doped film presents a plate-like grains with polycrystalline-like irregular grains. The size of the grains is larger (350 nm) and not uniform. Incorporation of tin extinguishes the blue-green band while appears a blue light at λ = 465 nm and increases the value of the band-gap transition. The presence of tin in the material leads to great luminescent spots, due to large grain sizes.	[190]
5 at% Sn-doped ZnO thin film with 0.2 M	Spray pyrolysis	The thin films have (002) as the preferred orientation. X-ray diffraction patterns confirm that the films have polycrystalline nature. The grain size values of Sn-doped ZnO thin films calculated from XRD are found to be 39.5 nm. The optical band gaps	[191]

solution of zinc acetate dehydrate and tin chloride dihydrate used as precursors		of the films were determined to be approximately 3.295 eV. The inclusion of dopant into films expands also width of localized states as E_U = 269 meV. The refractive index dispersion curves obey the single oscillator model. The dispersion parameters and optical constants of the films were determined. These parameters changed with Sn dopant.	
Sn:ZnO thin films with different Sn concentrations of 0.1, 1 and 10 at%	Pulsed laser deposition (PLD)	The high-quality (001) oriented thin films, grown on single-crystal Si (001) substrates. Roughness and topography were studied by using an atomic force microscope (AFM), the images show a smooth surface with a mean square roughness within the 4 to 6 nm range for all different Sn concentrations. Only films with a nominal 0.1 at% Sn exhibit an improvement of the transport properties, lower resistivity and higher donor concentration, with respect to pure ZnO thin films. For films with larger Sn nominal concentrations segregated SnO_2 and Sn_2ZnO_4 phases appear that lead to larger film resistivities and no increase in donor concentration. The 0.1 at% Sn-doped film is accordingly a good candidate to study how n-doping	[193]

		affects the possible room temperature ferromagnetism when co-doping with Mn.	
Sn-doped ZnO thin films with zinc acetate dehydrate and tin tetrachloride (with Sn/Zn=0, 1, 2, 3 and 5 at%.)	Sol-gel	The XRD patterns of the ZnO:Sn films that were prepared without the formation of a secondary phase, such as SnO_2 and the 5 at% Sn-doped ZnO thin film, show high (002) peak intensities; this indicates such films exhibit *c*-axis preferred orientation. The calculated average crystallite sizes of undoped and 1 at% Sn-doped ZnO thin films were 13.0 and 10.0 nm, respectively. When the Sn concentration increased from 2 to 5 at%, the average crystallite size decreased about 8.2–8.8 nm. The plane view of an SEM micrograph of an annealed undoped ZnO film shows fiber-like streaks or wrinkles. The bandgaps calculated from transmittance spectra increased from 3.23 to 3.27 eV as the Sn dopants increased from 0 to 5 at%. Undoped film exhibits a resistivity of 2.4×10^2 Ω-cm and the resistivities of 1, 2 and 5 at% Sn-doped ZnO thin films were 3.4×10^2, 9.3×10^2 and 9.0×10^2 Ω-cm, i.e. when the Sn concentration increased from 2 to 5 at%, the resistivity of film scarcely changed. The results show that Sn-doped ZnO thin films demonstrate obviously improved surface	[194]

		roughness, enhanced transmittance in the 400–600 nm wavelength range and reduced average crystallite size. Among all of the annealed ZnO-based films in this study, films doped with 2 at% Sn concentration exhibited the best properties, namely an average transmittance of 90%, an root mean square (RMS) roughness value of 1.92 nm and a resistivity of 9.3×10^{2} Ω-cm.	
Sn-doped ZnO thin films using zinc acetate dihydrate and $SnCl_4$ as precursors (with 2% of Sn concentration)	Sol-gel	Crystallite size from XRD of pure ZnO revealed 36 nm in (100) plane. The average size of crystallites was calculated from the effective-mass model, the value found was 22.87 nm which is in agreement with the value given by XRD. In UV-visible spectroscopy, Sn dopant reduces the band gap until 3.30 eV for a doping rate of 7%.	[195]

A.2 Literature reviews of Sn-doped ZnO particles

Materials	Method	Conclusion	Reference
Sn-doped ZnO nanobelts with a mixture of ZnO and Sn powders (at a mass ratio of 10:1) acting as the precursor	Chemical vapor deposition (CVD)	From SEM images, these nanobelts have a width of about 80−120 nm, a thickness of about 15 nm, and a length up to a few tens of micrometers. The planar defects in the nanobelts include both antiphase boundaries (APs) and inversion boundaries (IBs), which may result from the minimization of structural strains. The introduction of Sn atoms might result in a rearrangement of the order of surface energies among $\{0001\}$, $\{01\bar{1}0\}$ and $\{2\bar{1}\bar{1}0\}$ surfaces, causing the nanobelts to grow along the $\langle 01\bar{1}0\rangle$ direction. The NBE emission peak at 3.24 eV for Sn-doped ZnO nanobelts becomes broader and slightly shifts to a lower energy, compared with the emission of undoped ZnO nanowires, which are attributed to the introduction of Sn into the nanobelts.	[80]
Sn-doped ZnO	Microwave	The XRD diffraction peaks of the pure ZnO are sharp and intense, revealing the	[87]

nanoparticles using zinc acetate dehydrate and $SnCl_2 \cdot 2H_2O$ as precursors	heating	highly crystalline character of the ZnO sample, while the diffraction peaks of the Sn-doped ZnO are broad and weak, indicating a small crystal size or semicrystalline nature of this sample. The specific BET surface areas of pure and Sn-doped ZnO revealed 4.0 and 3.8 m^2/g, respectively. From SEM images, the shape of the prepared pure ZnO photocatalyst looks like rice and with average particle size of about 100nmin diameter and 300 nm in length. The shape of the prepared Sn-doped ZnO looks like diamond and with average particle size of about 300 nm. Although the pure ZnO show a smaller particle size than the Sn-doped ZnO photocatalyst. From UV-vis absorption results, the prepared pure ZnO and Sn-doped ZnO photocatalyst had a broad absorption band from ultraviolet to visible region and the absorbance of the photocatalyst slightly decreases as the wavelength increases, which indicate that the prepared ZnO photocatalyst has a potential capacity of photocatalytic activity utilizing sunlight. The diffuse reflectance spectroscopy (DRS) spectra of Sn-doped ZnO showed that the curve has a clear absorption in the visible range, beside the absorption edge near 400 nm. Photoluminescence (PL) spectrum of	

		the prepared pure ZnO and Sn-doped ZnO photocatalyst were similar, only one broad luminescence band covered from 430 to 550 nm, which can be assigned to blue-green regions, but the PL intensity were different (the PL intensity of Sn-doped ZnO was lower than undoped ZnO). The sunlight photocatalytic activity of the prepared pure ZnO and Sn-doped ZnO photocatalyst was investigated by the degradation of Methylene Blue (MB) solution under sunlight irradiation. Compared with pure ZnO, 13% higher decolorization rate and 29–52% higher mineralization efficiency were obtained by the Sn-doped ZnO. The results indicated that Sn-doped ZnO had a higher photocatalytic activity and Sn dopant greatly increased the photocatalytic activity of ZnO.	
Sn-doped ZnO nanobelts (with Sn concentrations in the range of	Chemical vapor deposition	X-ray diffraction and Raman spectra showed that the Sn-doped ZnO nanobelts have wurtzite structure at low Sn concentration (<2.1 at%) and over 2.1 at% a part of them starts to have the inverse spinel Zn_2SnO_4 structure phase. In SEM images, their length has several tens of micrometers and the widths are in the range of 180–600	[177]

0.7−12.3 at%)		nm. The shape and size of the nanostructure have no obvious change under the different Sn-doped concentrations. In addition, for Sn-doped ZnO nanobelts, the photoluminescence spectra indicate that ultraviolet emission peak appears first a blue shift with the increase of Sn concentration due to Burstein-Moss effect and then exhibits a red shift due to band gap renormalization effect.	
Pure and Sn-doped ZnO nanostructures with using a mixture of Zn and Sn metal powders in a weight ratio of 80:20	Thermal evaporation	Pure and Sn-doped ZnO show nearly same crystallite size, viz. 38 nm and 31 nm respectively, as calculated by using the Scherrer formula. The SEM images of pure ZnO show interwoven wires/ribbons forming bundles, while Sn-doped ZnO depicts formation of the star shaped, and tetrapods along with the isolated rods having sharp tips. The EDX of Sn-doped ZnO indicates presence of 44 wt% Sn which is quite higher than the initial precursors concentration (i.e. 20 wt%). The responses towards different gases (acetone, ethanol, LPG, DMA, H_2 and HNH3) for pure and Sn-doped ZnO were recorded at 275°C for 500 ppm of their concentrations. Pure ZnO shows high response (%S = 800) and selectivity towards acetone vapors while all other	[183]

		reducing gases show sensitivity less than 300. In contrast, the Sn doping does not improve gas sensitivity or selectivity towards any gas. It shows nearly similar response (%S = ~120) towards all gases including acetone, indicating that incorporation of Sn does not improve gas sensitivity and losses the selectivity. The response time for ZnO towards 500 ppm of acetone vapor is nearly a minute while the recovery time is ~2 min. On Sn doping the PL spectrum shows only one strong broad peak at 517 nm, which corresponds to the green emission and is generally accepted to be, due to the emission from a deep-level or trap-state emission.	
Sn-doped ZnO particles using ZnO (Union Minière Oxyde-La Ciotat; SSA_{BET}=44 m^2/g)	Impregnation	This work demonstrated that the hydrogenation of methyl oleate into oleyl alcohol can be performed in the presence of CoSn/ZnO catalysts. It was observed that the Sn/ZnO catalyst is less active than CoSn/ZnO and Co/ZnO catalysts. The strong adsorption of oleyl oleate over the Sn/ZnO catalyst can also inhibit the activation of hydrogen. The Sn/ZnO catalyst favors the formation of unsaturated alcohols (UAs), even if the oleyl oleate is the major product of the reaction.	[196]

and $SnCl_2.2H_2O$ (Fluka) as raw materials			
Tin particle guided growth of ZnO nanowires/ nanobelts	Vapor-liquid-solid (VLS)	Tin catalyst not only can guide $[0001]$ growth nanowires, but it also can guide $[01\bar{1}0]$ and $[2\bar{1}\bar{1}0]$ growth nanobelts. The orientation relationship between the $[0001]$ growth ZnO nanowire and the single crystal β phase Sn particle is $(020)\,\mathrm{Sn} \parallel (0001)\,\mathrm{ZnO}$, $[1h1]\,\mathrm{Sn} \parallel [21h1h0]\,\mathrm{ZnO}$. For nanobelts growing along $[01\bar{1}0]$ and $[2\bar{1}\bar{1}0]$, the orientation relationships are $(200)\,\mathrm{Sn} \parallel (01\bar{1}0)\,\mathrm{ZnO}$, $[020]\,\mathrm{Sn} \parallel [0001]$ ZnO and $(002)\,\mathrm{Sn} \parallel (2\bar{1}\bar{1}0)\,\mathrm{ZnO}$, $[020]\,\mathrm{Sn} \parallel [0001]\,\mathrm{ZnO}$, respectively. One tin particle can initiate the growth of two 1D nanostructures; the tin particle is single crystal after growth, and it preserves epitaxial relationships with the grown nanostructures.	[197]
ZnO nanowires	Thermal	The nanowires consist of single-crystalline wurtzite ZnO crystal, and the average	[198]

doped with a high concentration of Sn (~15%).	evaporation	diameter is 80 nm. The growth direction of vertically aligned Sn-doped nanowires is $[010]$. For the growth of Sn-doped ZnO nanowires, the temperature range of 900−1000°C was used. At the temperatures above 1000°C, the formation of SnO_2, and spinel typed Zn_2SnO_4 alloy nanowires takes place. The HRTEM images and selected area electron diffraction (SAED) patterns confirm that all ZnO nanowires consist of single crystalline wurtzite ZnO crystal. The EDX and XPS data reveal that the average content is as high as about 15%, and the Sn-doped nanowires show the Sn 3d3/2 and Sn 3d5/2 peaks located at 494.8 and 486.8 eV, whose gap between two peaks is 8.0 eV that is consistent with the reference value of element, 8.41 eV, respectively. The Sn doping causes the largest XRD peak broadening, most significant E_g reduction, and strong green emission, which would be due to the largest charge density of Sn. It suggests that the charge density of doped element would be an important parameter in controlling the optical properties of ZnO nanowires. The UV-visible absorption spectrum reveals the E_g decrease that would	

		be originated from the localized band edge states at the doping sites. The peak position of the Sn-doped nanowires shifts to the lower energy 3.25 eV. In particular, the Sn-doped nanowires have a green emission band around 2.5 eV that originates from the recombination of the holes with the electrons occupying the singly ionized O vacancies. The largest charge density of Sn will give rise to more defects such as oxygen vacancies, which result in the great enhancement of green emission. It shows the near-band-edge (NBE) peak at around 3.24 eV, the broader width caused by the doping, and the enhanced green emission for the Sn doping, which are all consistent with the results of PL.	
Doping of ZnO bulk ceramics with small amounts of tin oxide using	Highly reactive co-precipitation	An improvement of the semiconductor behavior of ZnO is also necessary to obtain good electrical properties and in this way tin oxide is expected to increase the electrical conductivity of bulk ZnO, as it is assumed to act as a doubly ionized donor. However, the range of solid solution of tin into ZnO lattice is found to be limited as it rapidly segregates to form secondary phases. Concentrations as low as 0.1 mol% of	[199]

$Zn(CH_3COO)_2 \cdot 2H_2O$ and $SnCl_4 \cdot 5H_2O$ as precursors (with ZnO-based compositions containing 0.1, 1 and 10 mol% of SnO_2)		SnO_2 lead to the formation of a spinel-type phase whose presence yields a non-linear electrical response that hinders the donor effect of tin oxide. This phase is formed gradually from the reaction between ZnO and SnO_2, and no trace of the $ZnSnO_3$ phase is ever detected. The system doped with 0.1 mol% of SnO_2 shows an improvement of the electrical conductivity of bulk ZnO. Nevertheless, such a low range of solid solution, which is practically at the impurity level, limits the application of this system in bulk ceramics. Better results should be expected in the form of thin film devices, where it could be a good semiconductor candidate to obtain room temperature ferromagnetic semiconductor materials, once doped with Mn or other magnetic elements.	
Single crystalline Sn-doped ZnO nanobelts which ZnO, SnO_2 and C	Carbon thermal reduction deposition	SEM-EDS and TEM analyses showed that the Sn-doped ZnO nanostructures contained a belt-like morphology have the high aspect ratio with the lengths varying from several microns to hundreds of micron, the widths from tens to hundreds of nanometers, and the thickness for most nanobelts was below 100 nm, with Sn doping	[200]

powders with a purity of 99.9% (nZnO:nSnO:nC= 5:1:6) used in this process		content about 1.9%, and the nanobelt has a regular geometric shape with a smooth surface and uniform width of 40 nm along the growth direction of nanobelts was along the $[0001]$ direction, respectively. A weak UV emission peak at around 398.4 nm and the strong green emission peak at around 494.8 nm were observed at room temperature. The results revealed that properly doped ZnO nanostructures could be very useful for their promising applications in the fields of micro/nano-structured functional devices.	
Single crystalline Sn-doped ZnO nanowires	Simple thermal evaporation approach without introducing any catalysts	The XRD investigation confirmed that the products were of the wurtzite structure of ZnO. The intensity of the ZnO (002) peak is much stronger than other ZnO peaks, suggesting the (002) crystal face might be the primary face of the nanowires. This can be further confirmed by HRTEM and the corresponding SAED. From SEM images, these doped nanowires have diameters in the range 30−50 nm and lengths of several tens of micrometers with growth direction along the *c*-axis of the crystal plane. On TEM analysis, the separated spacing between the adjacent lattice fringes of	[201]

		0.52 nm indicated by parallel lines corresponding to ZnO crystal d-spacing, which indicates that the single crystalline Sn-doped ZnO nanowires grew along the [001] direction. Further quantitative analysis reveals that the Sn content in the ZnO nanowires is about 6.5 at%. Photoluminescence of these doped nanowires exhibits a weak ultraviolet (UV) emission peak at around 400 nm and the strong green emission peak at around 495 nm at room temperature, which may be induced by the Sn-doping.	
Sn-doped (1.8, 7.4 and 3.4 mol% respectively) and pure ZnO using $Zn(Ac)_2 \cdot 2H_2O$ and $SnCl_2$ (10 mol% of Sn) as	Hydro-thermal method	From XRD pattern and Raman spectra, Ti and Sn dopants lead to a secondary phase besides ZnO crystal. The mean crystallite diameter (d_{101}) of ZnO and Sn-ZnO can be estimated to be 23 and 21nm respectively, from Scherrer's formula. SEM observation shows polycrystalline of the particles instead of single crystal. Under UV-vis spectra, Sn-ZnO keeps unchanged compared with pure ZnO. The gas sensing property is studied using formaldehyde in air with the concentrations in the range of 0−205 ppm and working temperatures of 200, 300 and 400°C. The results show that the	[202]

precursors		maximum response of pure ZnO to 205 ppm formaldehyde is ~43 (at relative humidity 70±10%) at 400°C. But the gas response maxima shift to 300°C for Sn-ZnO is ~140 at 205 ppm). Beyond the maxima, the response of Fe-ZnO is lower than that of pure ZnO, while that of Sn-ZnO is always higher. The response time, defined as the time for sensor to get 90% of the signal, is ~10 min at 200°C and ~1 min at 300 and 400°C. The PL spectra are decomposed to distinguish the donor-related (DL) and acceptor-related (AL) subpeaks. And the higher DL content and lower AL content might account for the enhanced gas sensing property of doped ZnO, especially Sn-ZnO. The secondary phase and the PL subpeak contents might the dominant two aspects of the doping effect on gas sensing property of ZnO.	
Sn-doped ZnO (SZO) microrods	Thermal evaporation	From XRD measurements The sample exhibited a common exactly wurtzite hexagonal crystallized of ZnO and no peaks for tin oxide or other impurities were detected, revealing the phase purity of the products. The morphologies and composition of as-prepared products examined by SEM and EDX, respectively, gives	[203]

		the general morphologies of the SZO microrods grown in [0001] direction and constructed from slips perpendicular to the growth direction. The SZO contains lots of quasi one-dimensional microstructures, which are about dozens micrometers in length and ~1.5−2.0 μm in width. From EDX analysis, the concentration variation range of these microrods is 0.4%–1.3%. Photoluminescence (PL) of these SZO microrods exhibits a weak ultraviolet (UV) emission peak at around 382 nm and the strong green emission peak at around 525 nm at room temperature. Field emission measurements demonstrate that the SZO possess good performance with a turn-on field of ~1.94 V/μm and a threshold field of ~3.23 V/μm, which have promising application as a competitive cathode material in FE microelectronic devices.	
Sn-doped ZnO and pure ZnO using $ZnSO_4 \cdot 7H_2O$ and	Co-precipitation	From SEM images, Sn-ZnO has a similar morphology of 20–80 nm. The XRD patterns of pure and doped ZnO reveal that all ZnO nanoparticles belong to wurtzite phase, with no other phase related to the oxide of the dopants. The mean crystallite diameter along [101] direction could be estimated from XRD to be ~33 and ~12 nm	[204]

$SnCl_2$, $Ni(NO_3)_2$ as precursors (at different concentrations of 0.2, 0.5, 2.2, 5 and 10 mol%)		for ZnO and Sn-ZnO, respectively. The gas sensing property is studied using formaldehyde in the concentration range of 0−205 ppm and working temperatures in the range of 0−500°C. Their formaldehyde gas sensing properties are evaluated and the results show that 2.2 mol% Sn dopant can increase the response of ZnO by more than 2 folds (~140 at 200°C), while other dopants increase little response or even decrease response. Further, CdO is used to activate ZnO based formaldehyde sensing material. It is demonstrated that 10 mol% CdO activated 2.2 mol% Sn-doped ZnO has the highest formaldehyde gas response (~2000), with a linear sensitivity of ~10/ppm at lowered work temperature of 200°C than 400°C of pure ZnO, and high selectivity over toluene, CO and NH_3, as well as good stability tested in 1 month.	
2 wt% Sn-doped ZnO nanobelts (NBs)	Thermal evaporation	From XRD patterns, intensities for the peaks of (100) and (101), increase abruptly while the intensity for the (002) peak reduces tremendously after doping with Sn. From FESEM images, the undoped ZnO nanostructures (NSs) present as wires-like structures while belts shape of NSs were found in the Sn-doped ZnO. The NBs	[205]

		formed have the average width of about 300 nm and the thickness of about 25 nm. The optical band gap of both undoped ZnO nanowires and Sn-doped ZnO nanobelts changes from 3.26 eV to 3.13 eV. The Sn dopant can narrow down its band gap and enhance the electrical conductivity of ZnO nanostructure. This result confirms that the cationic doping (Sn) in ZnO can be accomplished effectively by this process. The Si-(Sn-doped ZnO NBs) exhibits great p-n junction behavior. These Sn-doped ZnO NBs may be applied as a good gas and also photo detectors.	
Tin-doped ZnO nanocrystals (with Sn concentrations of 0−20 wt%) using zinc nitrate hexahydrate and	Room temperature solid-state reaction	XRD patterns revealed that no other phases such as the often seen $Zn(OH)_2$, SnO_2 or Zn_2SnO_4 were detected. The diffraction peaks of tin-doped ZnO shifted to lower angles. The gas sensing property is studied using ethanol vapor, acetone, ammonia, carbon monoxide, gasoline and toluene in air, in the concentration range of 10−1000 ppm and working temperatures in the range of 200−320°C. The materials showed a high gas response to ethanol vapor, and the gas response can reach a maximum of R_a/R_g = 124. In addition, tin-doped ZnO materials exhibited improved photocatalytic	[206]

stannic chloride pentahydrate as precursors		performance under over UVB irradiation toward methyl orange (MO) solution under a current density of 0.03 mg/l comparison with undoped ZnO.	
Sn-doped ZnO nanorods (with Sn concentrations of 1.0 mol%, 3.0 mol%, 5.0 mol%) using as $Zn(NO_3)_2.6H_2O$ and $SnCl_4$ as precursors	Hydro-thermal route	XRD patterns revealed that no peaks corresponding to SnO_2 crystals or other Sn phase were detected at Sn-doped ZnO samples. The total amount of Sn in ZnO was determined by inductively coupled plasma optical emission spectroscopy (ICP-OES) and was found that the atomic ratio of Sn/Zn was to be about 0.0, 0.0097, 0.0295, 0.0497, which is close to the experimental dopant concentration. BET specific surface areas of pure ZnO and, 1.0, 3.0 and 5.0 mol% Sn-doped ZnO were 80.8, 80.1, 81.6 and 81.2 m^2/g. From UV-vis diffuse reflectance spectra, it can be seen that the band gap slightly decreases from E_g = 3.07 eV to 3.05 eV with increase in Sn concentrations from 1 to 3 mol%, respectively, even though the size of the as-synthesized samples remains unaltered. Solid state NMR result confirms that Sn^{4+} was successfully incorporated into the crystal lattice of ZnO. Room temperature	[207]

		photoluminescence showed that all the as-synthesized products exhibited a weak UV emission (380 nm) and a strong visible emission (540 nm), but the intensities of the latter emission increased with increase in Sn concentration. The improvement of visible emission at 540 nm in the Sn-doped ZnO samples was suggested to be a result of the lattice defects increased by doping of Sn in zinc oxide. The improvement of visible emission at 540 nm in the Sn-doped ZnO samples was suggested to be a result of the singly ionized oxygen vacancies (V_O^+) defects becoming higher. The lattice defects caused by Sn doping could serve as favorable trap sites of the electrons or holes to reduce their recombination and consequently increase the photocatalytic activities. Furthermore, the photocatalytic studies indicated that Sn-doped ZnO nanorods are a kind of promising photocatalyst in remediation of water polluted by some chemically stable azo dyes. The photocatalytic activity of the Sn-doped ZnO samples increases gradually with an increase of the Sn content (Sn(5.0 mol%)-doped ZnO > Sn(3.0 mol%)-doped ZnO > Sn(1.0 mol%)-doped ZnO > pure ZnO). In order	

		to investigate the defects coming from the surface or the bulk of the as-synthesized samples, photoluminescence spectroscopy of the as-synthesized Sn (3.0 mol%)-doped ZnO during an approximate process of photocatalytic conversion of methyl orange (MO) is measured. No obvious PL quenching of the as-synthesized Sn (3.0 mol%)-doped ZnO is seen when the approximate photocatalytic process occurs. Thus, it can be deduced that the change of PL intensity in our case is more a bulk effect than a surface phenomenon.	
Sn-doped ZnO nanorods (with Sn concentrations of 0−10 at%) using tin (stannous) 2-ethyl hexanoate and zinc	Flame spray pyrolysis	XRD patterns showed that Sn-doped ZnO, the (002) peak exhibits a dramatic reduction in intensity and pronounced broadening with increasing dopant content. In and Sn dopants, however, alter progressively the shape of the ZnO particles to a rod-like shape with increasing dopant concentration. Sn has a stronger nanorod-forming influence than In at low dopant levels. The driving force of nanorod formation with In and Sn as dopants is attributed to their higher valency and coordination relative to zinc and the associated disruption of crystal growth within the Zn plane. Sn-doped	[208]

naphthenate as precursors		ZnO shows that the crystallite size in the (002) plane decreases from 27 to 6 nm with the addition of only 4 at% dopant. The corresponding change in crystallite size for the (100) plane is 18 to 14 nm with 4 at% Sn dopant. The specific surface area increases steadily from 53 to 85 m^2/g as tin concentration increases from 0 to 6 at%. The 6 at% Sn-doped ZnO samples showed a similar increase in the crystallite size in the (100) plane from 12.1 nm (as prepared) to 16.0 nm (at annealing temperature of 700°C) and the crystallite size in the (002) plane changed from 4.4 (as-prepared) to 5.9 nm (annealing temperature of 700°C). Raman spectra for 0−10 at% Sn-doped ZnO found that each spectrum was normalized to the amplitude of the E2 mode (437 cm^{-1}) of the wurtzite. All Sn-doped powders exhibit two additional peaks at 570 and 670 cm^{-1}. These peaks are indicative of vibrations associated with the tin dopant atoms within the crystal, while the peak at 670 cm^{-1} is associated with a more highly coordinated structure than that of the 570 cm^{-1} peak.	

APPENDIX B

B.1 Photocatalytic calibration curve

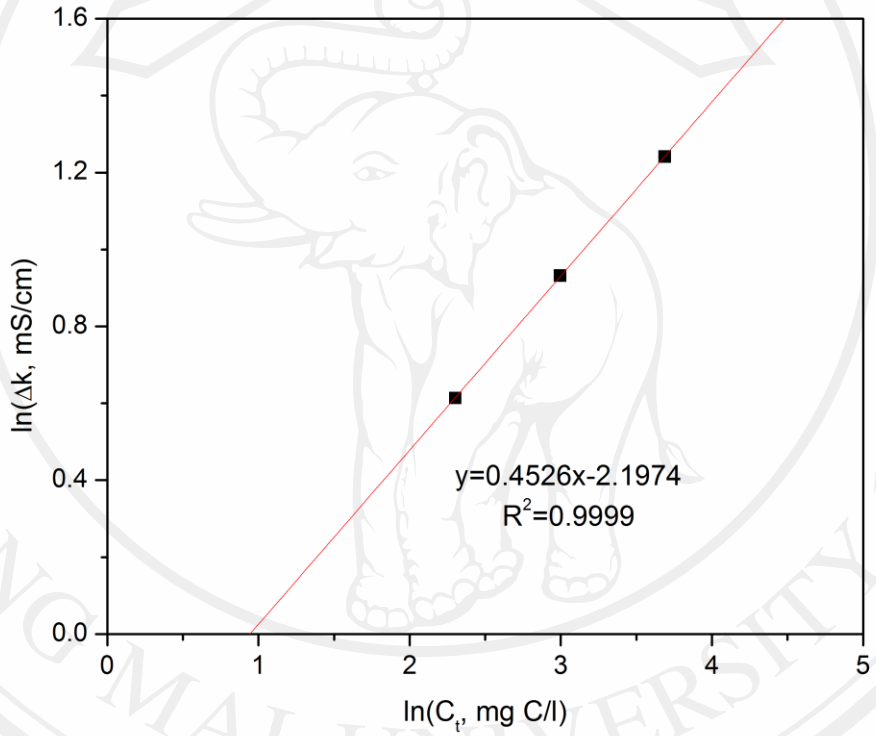

B.2 Repeated testing on phenol photodegradation

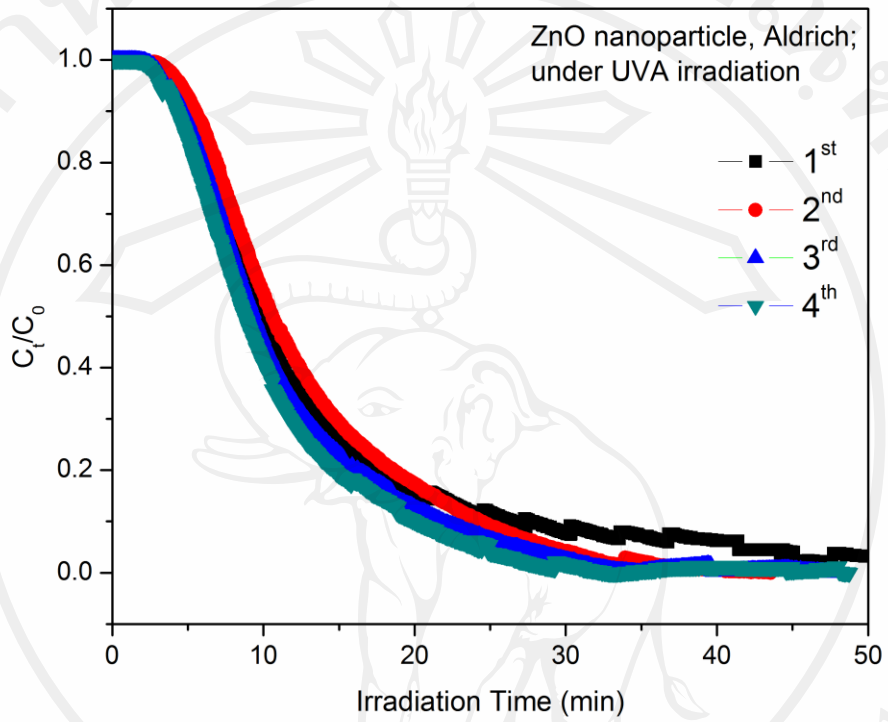

APPENDIX C

Peak Analysis

Data Set:[Book1]Sheet1!Undoped ZnO Date:17/11/2011

BaseLine:??WL

Chi^2=-- Adj. R-Square=-- # of Data Points=??WL

SS=-- Degree of Freedom=??WL

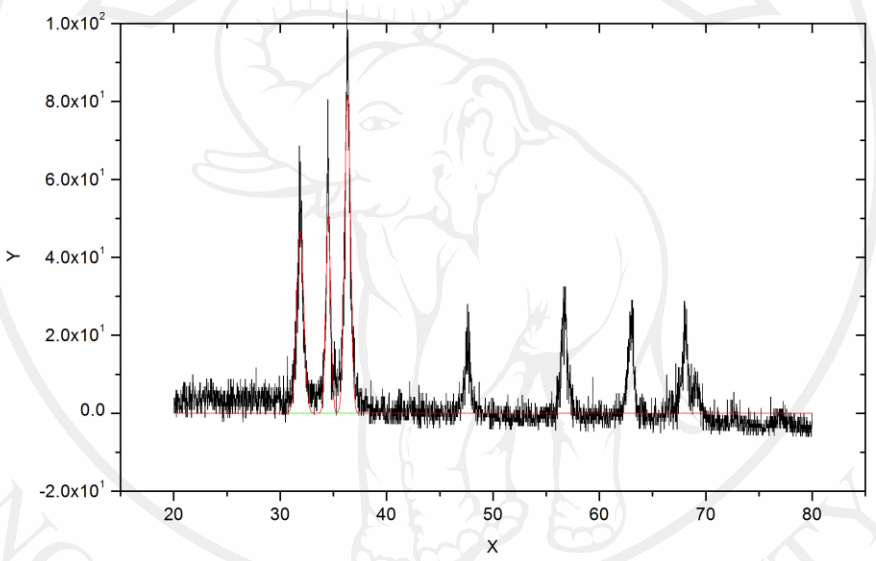

Fitting Results

Peak #	Peak Type	Area Intg	FWHM	Max Height	Center Grvty	Area IntgP
1	Gaussian	39.29361	0.79357	46.51609	31.87876	31.60137
2	Gaussian	29.3322	0.54115	50.92033	34.51859	23.59004
3	Gaussian	55.71566	0.64081	81.68064	36.33128	44.80859

Peak Analysis

Data Set:[Book1]Sheet1!0.5 atn-doped ZnO Date:17/11/2011

BaseLine:??WL

Chi^2=-- Adj. R-Square=-- # of Data Points=??WL

SS=-- Degree of Freedom=??WL

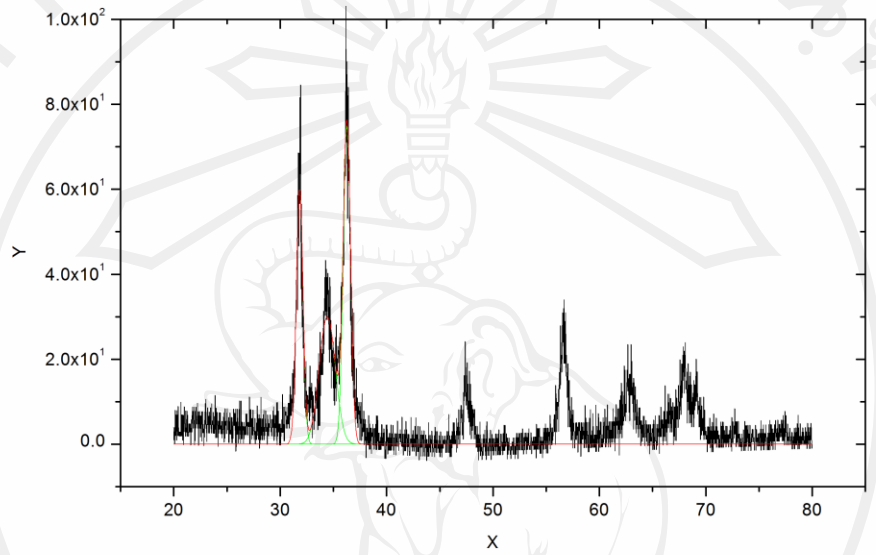

Fitting Results

Peak #	Peak Type	Area Intg	FWHM	Max Height	Center Grvty	Area IntgP
1	Gaussian	47.25922	0.74005	59.99198	31.81977	28.04382
2	Gaussian	56.41615	1.76924	29.95605	34.42656	33.47758
3	Gaussian	64.8438	0.81363	74.87017	36.26794	38.47859

Peak Analysis

Data Set:[Book1]Sheet1!1 atn-doped ZnO Date:17/11/2011

BaseLine:??WL

Chi^2=-- Adj. R-Square=-- # of Data Points=??WL

SS=-- Degree of Freedom=??WL

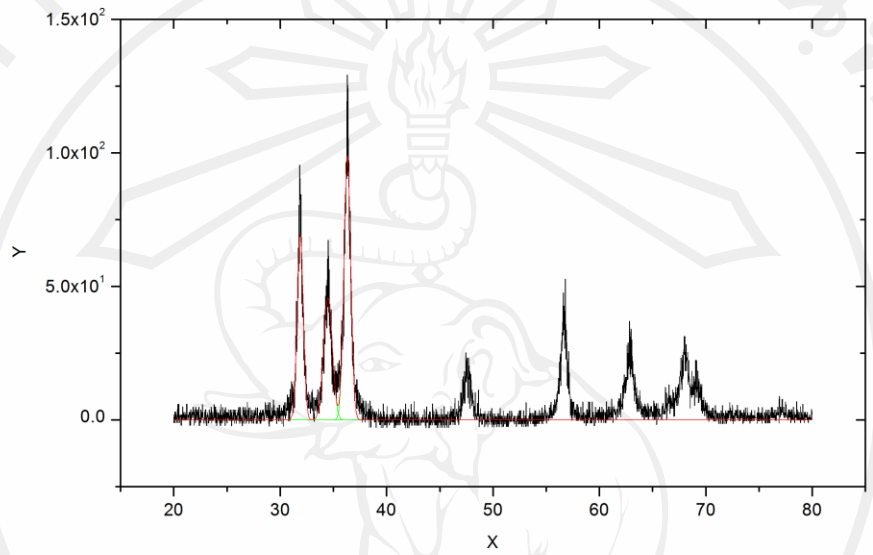

Fitting Results

Peak #	Peak Type	Area Intg	FWHM	Max Height	Center Grvty	Area IntgP
1	Gaussian	49.92642	0.67694	69.28683	31.88816	28.39804
2	Gaussian	46.68398	0.95949	45.70816	34.49268	26.55375
3	Gaussian	79.19898	0.75179	98.96647	36.31472	45.04821

Peak Analysis

Data Set:[Book1]Sheet1!2 atn-doped ZnO Date:17/11/2011

BaseLine:??WL

Chi^2=-- Adj. R-Square=-- # of Data Points=??WL

SS=-- Degree of Freedom=??WL

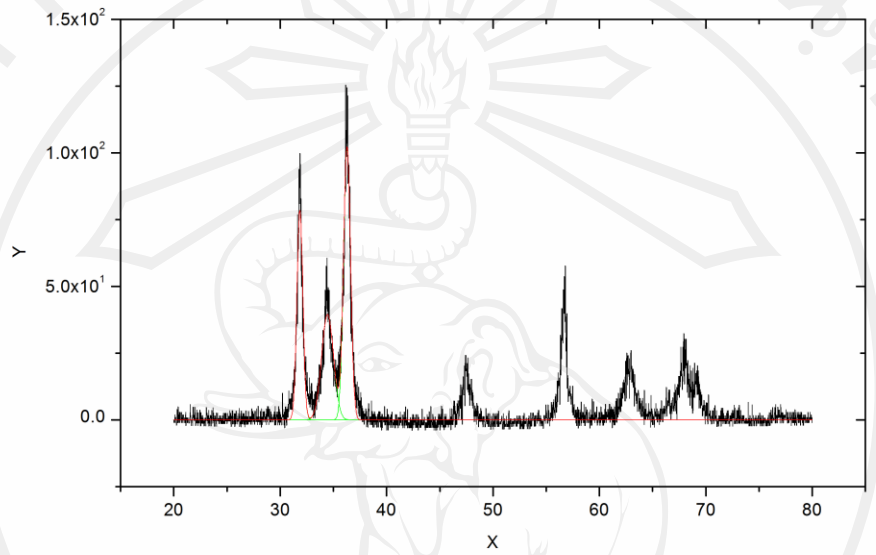

Fitting Results

Peak #	Peak Type	Area Intg	FWHM	Max Height	Center Grvty	Area IntgP
1	Gaussian	54.99994	0.65773	78.5565	31.85366	28.41212
2	Gaussian	55.22166	1.31258	39.52303	34.45417	28.52665
3	Gaussian	83.35758	0.76607	102.22231	36.28538	43.06123

Peak Analysis

Data Set:[Book1]Sheet1!3 atn-doped ZnO Date:17/11/2011

BaseLine:??WL

Chi^2=-- Adj. R-Square=-- # of Data Points=??WL

SS=-- Degree of Freedom=??WL

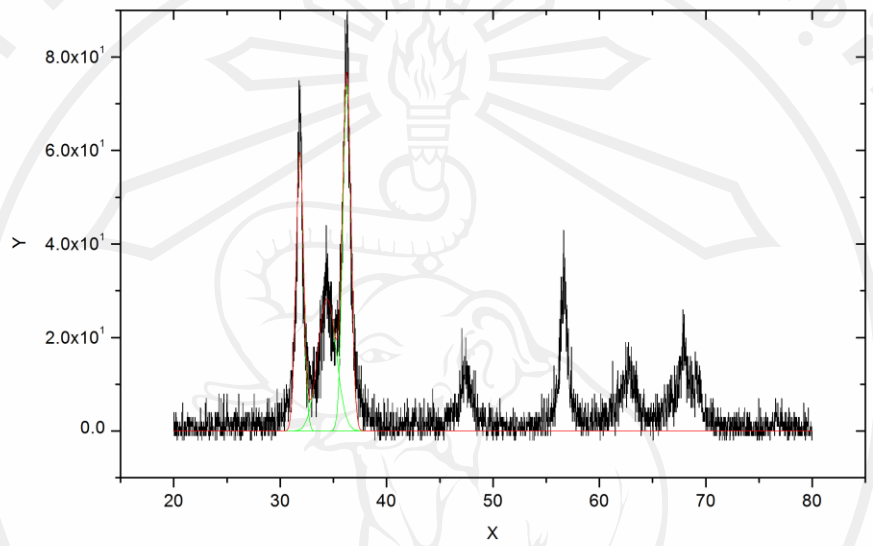

Fitting Results

Peak #	Peak Type	Area Intg	FWHM	Max Height	Center Grvty	Area IntgP
1	Gaussian	53.34915	0.84592	59.24713	31.84251	28.68125
2	Gaussian	60.96425	2.02816	28.2385	34.40452	32.77524
3	Gaussian	71.69364	0.90891	74.10164	36.27027	38.54351

Peak Analysis

Data Set:[Book1]Sheet1!5 atn-doped ZnO Date:17/11/2011

BaseLine:??WL

Chi^2=-- Adj. R-Square=-- # of Data Points=??WL

SS=-- Degree of Freedom=??WL

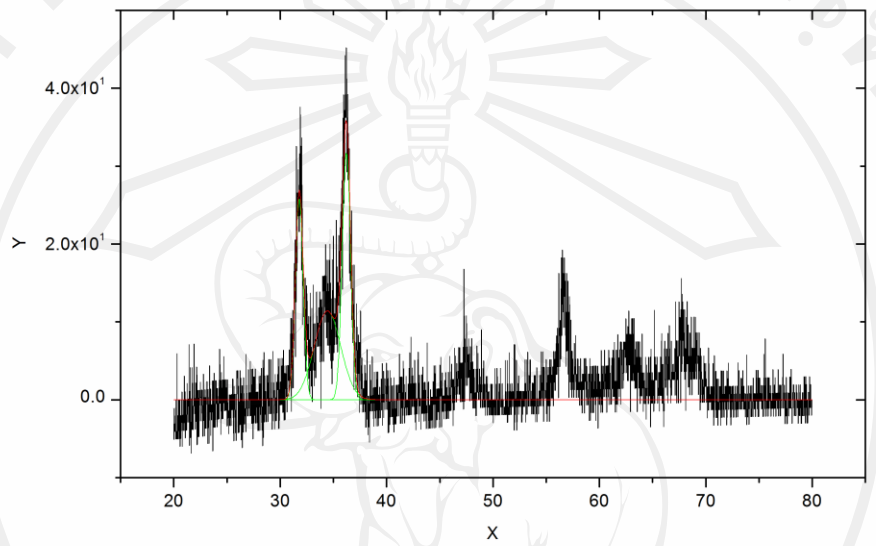

Fitting Results

Peak #	Peak Type	Area Intg	FWHM	Max Height	Center Grvty	Area IntgP
1	Gaussian	23.92209	0.87125	25.79432	31.79668	26.47642
2	Gaussian	35.44376	2.92271	11.39257	34.45106	39.22834
3	Gaussian	30.98659	0.91856	31.69096	36.22522	34.29525